A reduced-order model of a solid oxide fuel cell stack for model predictive control

L. van Biert[a*], P. Segovia Castillo [a], A. Haseltalab[a], R.R. Negenborn[a]

[a]*Department of Maritime & Transport Technology, Delft University of Technology*

[*]Corresponding author. Email: l.vanbiert@tudelft.nl

Synopsis

The maritime industry is actively exploring alternative fuels and drivetrain technology to reduce the emissions of hazardous air pollutants and greenhouse gases. High temperature solid oxide fuel cells (SOFCs) represent a promising technology to generate electric power on ships from a variety of renewable fuels with high efficiencies and no hazardous emissions. However, application in ships is still impeded by a number of challenges, such as low power density and high capital cost. Another challenge is the slow response to load transients. This is a result of conservative thermal management strategies needed to avoid excessive thermal stresses in the stack. Model predictive control may be used to enhance transient load response while ensuring sufficient thermal management, but require models that can be evaluated in real-time. Therefore, a reduced-order SOFC stack model is developed in this work and verified with a high fidelity model from previous work. In addition, a preliminary framework is provided for its application in model predictive control. The reduced-order model and control framework will be used in future work to optimise thermal management of SOFC stacks for improved transient response while respecting physical and operational constraints.

Keywords: Solid oxide fuel cell; Transient simulation; Thermal management; Reduced-order model; Model predictive control.

1 Introduction

The application of fuel cell technology on ships receives increasing attention, as they enable power generation from a variety of renewable fuels with high efficiencies and no hazardous emissions [12]. High temperature solid oxide fuel cells (SOFCs) enable particularly high electrical efficiencies of 60% and higher, but their application in shipping is still hindered by their relatively low power density and high cost [4, 8]. In addition, SOFCs struggle to follow rapid changes in power demand and thus need to be hybridised with engines or batteries to meet ship requirements [11].

In contrast to liquid-cooled low temperature fuel cells, SOFCs are typically cooled by providing an excess amount of air, which is primarily supplied as oxidant [3]. Air-cooling eliminates the need for a separate cooling system and enables recovering high temperature heat, but the relatively low volumetric heat capacity of air also results in large volumetric air flow rates, large temperature gradients or both [15]. Large volumetric air flows increase the parasitic consumption of the air blower. Large temperature gradients can be detrimental to the long-term operation of SOFCs, as they give rise to thermal stresses, which lead to the deformation and even failure of cell components or even cells.

Appropriate thermal management is important to operate SOFCs efficiently and reliably. However, it may take several minutes before the temperature profile within an SOFC stack stabilises following a load change. Therefore, the power ramp rate is usually limited to ensure that the thermal management system is able to adjust the air flow and avoid thermal overloading [2]. In practice, it may take up to an hour to ramp an SOFC system from idle operation to its rated power while ensuring the constrains on internal maximum temperatures and temperature gradients are respected.

There are various ways to enable faster load transients from an operational perspective. For example, the SOFC may be operated well within its operational limits such that sufficient margin for load transients is reserved, or temporary thermal overloading is tolerated. However, the first method would inevitably compromise the power output from the stack as it is not operated at the most favourable conditions, while the latter shortens the expected

Authors' Biographies

Dr.ir. Lindert van Biert is an assistant professor Marine Engineering at the Ship Design, Production and Operations section of the Maritime & Transport Technology department, Delft University of Technology. His research focusses on characterisation, modelling, simulation and application of power and propulsion systems based on fuel cells, and the adoption, storage and bunkering of renewable fuels.

Dr. Pablo Segovia is a postdoctoral researcher at the Maritime & Transport Technology department of Delft University of Technology (The Netherlands). His research interests include optimization-based control and state estimation approaches for large-scale and complex systems, with applications to water systems and transportation networks.

Dr. Ali Haseltalab is specialized in control and design for powertrains and is currently working at FEV NL/Europe. He received his PhD from Delft University of Technology in 2019, where he studied control for autonomous ships with DC power and propulsion systems. He has worked towards the integration of novel energy sources into powertrains of vehicles and marine systems in several research and engineering projects.

Prof.dr. Rudy Negenborn is full professor in Multi-Machine Operations & Logistics. He is head of the Section Transport Engineering & Logistics of Department Maritime & Transport Technology, and leads the Researchlab Autonomous Shipping. His research interests include automatic control and coordination of transport technology (including autonomous vessels), with a focus on multi-agent system and model predictive control approaches that benefit from real-time information and communication potential.

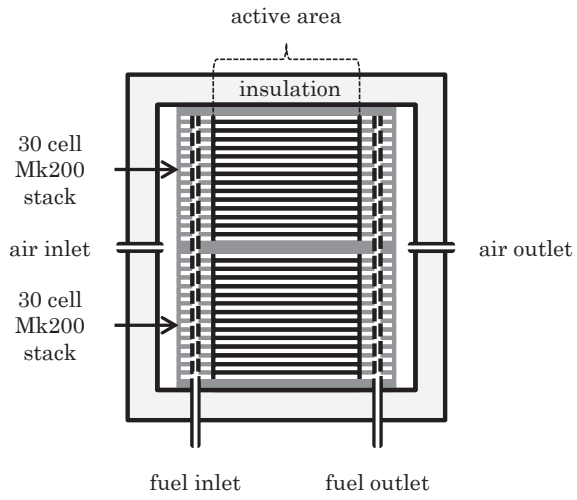

(a) Sunfire ISM.

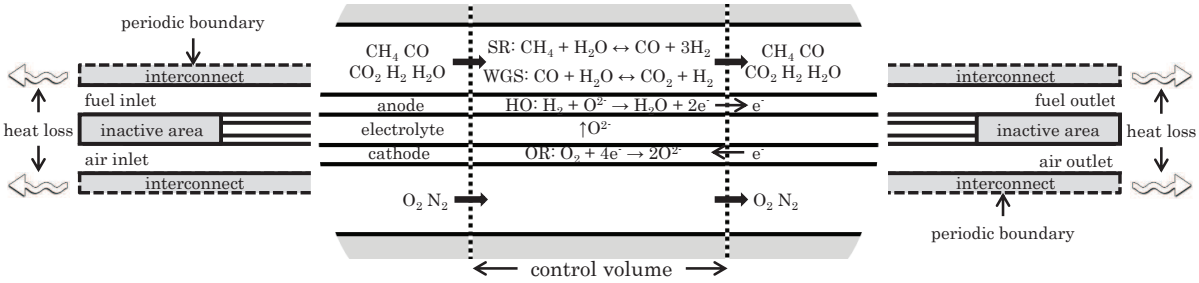

(b) 1D stack model overview.

Figure 1: Schematic overview of the Sunfire ISM and the full stack model, reproduced from [14].

lifetime of the stack. Alternatively, thermal management of the SOFC may be improved, for instance by adopting a secondary coolant or enhance internal heat transfer. Thermal management may also be improved through advanced control methods.

State-of-the-art commercial SOFC systems rely mostly on well-established feedback control. While this provides robust and reliable thermal management, feedback control only is inherently lagging behind event and does not exploit intrinsic knowledge of the system and upcoming events. For SOFCs, this issue is exacerbated by the long stabilising times induced by the large thermal mass. Consequently, power modulation is limited considerably to ensure sufficient time for a feedback controller to adjust the air flow following the sluggish thermal response of the system. In contrast, model-based control methods make use of the known system behaviour, allowing pro-active control actions. As such, they may enable faster modulation of system inputs and, consequently power output.

Implementing model predictive control requires models that can be run in real-time with limited computational demand. Therefore, a reduced-order model (ROM) of an SOFC stack is developed in this study for model-based control. The ROM is based on a simplified physical model of the SOFC stack, complemented with an area specific resistance (ASR) which is fitted to a high fidelity model developed in previous work [13]. The ROM is subsequently verified with the high fidelity model and simulation experiments. Finally, a preliminary framework for its use for model predictive SOFC control is provided.

2 Reduced-order model description

A full dynamic SOFC model was developed in previous work [13]. While the model can be used for any SOFC stack type through modification of the geometric data and material properties, the model presented in [13] was parameterised for the integrated stack module (ISM) developed by Sunfire GmbH and validated with both cell experiments and manufacturer data for steady-state operation. This high fidelity model is spatially discretised along the flow direction and solves dynamic mass and energy balances for the fuel, air, electrochemical cell and interconnect separately. A schematic overview of the Sunfire ISM and full stack model are shown in 1. The ROM developed in this work is based on the same SOFC stack model and assumptions, but simplified substantially.

The ROM follows a lumped parameter approach and only accounts for the dynamics in the stack temperature, while all other balances are assumed to be quasi-static. In other words, the dynamics of the electrochemistry, mass flows, chemistry and charge are assumed to be infinitely fast. This assumption is reasonable since the model is developed for thermal management purposes. As a result, the number of dynamically modelled states is reduced to a single one, while the high fidelity model consists of a numerically stiff, highly non-linear system of equations comprising 960 dynamic states, 12 for each discretisation unit. Consequently, the model runtime is reduced dramatically and suitable for (faster than) real-time simulations.

The temperature and partial pressure vary from inlet to outlet, both in practice and in the high fidelity model. Since the ROM is lumped and spatial variations are ignored, the properties can be either taken at the inlet, outlet or averaged. In this work, the SOFC is modelled as a continuously stirred tank reactor, in analogy to [5]. Consequently, the average stack temperature and the partial pressure of species i are assumed equal to the outlet conditions:

$$T^{\text{stack}} = T^{\text{out}} \tag{1}$$

$$p_i^{\text{stack}} = p_i^{\text{out}}. \tag{2}$$

For the co-flow design of the stack considered, this modelling assumption results in an overestimation of the stack temperature and steam partial pressures, and an underestimation of the hydrogen and oxygen partial pressure. Both contribute to an underestimation of the Nernst voltage according to (14). However, since the operational voltage should be below the Nernst voltage, other choices could theoretically give thermodynamically unfeasible operational voltages, while this choice inherently respects this physical constraint. Moreover, the resulting numerical error should be compensated by appropriate determination of the ASR.

2.1 Energy balance

The differential equation describing the dynamics of the stack or outlet temperature follows from the stack energy balance:

$$\frac{\partial T^{\text{stack}}}{\partial t} = \frac{\partial T^{\text{out}}}{\partial t} = \frac{1}{\bar{c}_{p,\text{stack}}} \left\{ \sum_i \left(\dot{n}_i^{\text{in}} h_i(T^{\text{in}}) - \dot{n}_i^{\text{out}} h_i(T^{\text{out}}) \right) - I_{\text{stack}} U_{\text{stack}} - \dot{Q}_{\text{loss}} \right\} \tag{3}$$

The heat capacity of the stack, $\bar{c}_{p,\text{stack}}$, is estimated by adding the heat capacities of the individual solid components. Assuming a linear temperature profile, the heat capacity is then divided by two in (3), as the temperature at the outlet of the stack changes two times faster than the average stack temperature. The inlet flows of fuel and air $\dot{n}_i^{\text{in}}$ are an input to the model, while the outlet flows $\dot{n}_i^{\text{out}}$ follow from the mass balance described in 2.2. The specific enthalpy of species i, $h_i(T)$, is calculated using the Shomate equation with coefficients provided by the National Institute of Standards and Technology Chemistry WebBook [7, 10].

The stack current I_{stack} is an input to the model and the resulting stack voltage U_{stack} is calculated using the electrochemical equations presented in Section 2.3. Although the electrochemistry is simplified substantially in the ROM, it does depend on the stack current, stack temperature as well as fuel and air flow, thus giving rise to highly nonlinear behaviour. Finally, the heat loss to the environment is calculated using Newton's law of cooling

$$\dot{Q}_{\text{loss}} = \lambda (T^{\text{stack}} - T^{\text{amb}}), \tag{4}$$

assuming an ambient temperature T^{amb} of 25°C. Similar to the high fidelity model, the heat transfer coefficient λ is determined based on the experimental data reported by Kluge et al. [6].

2.2 Mass balance

The mass balance accounts for the chemical and electrochemical reactions, assuming quasi-static behaviour:

$$\dot{n}_i^{\text{out}} = \dot{n}_i^{\text{in}} + \sum_m \nu_{i,m} r_m \tag{5}$$

with $\nu_{i,m}$ the stoichiometry of species i in reaction m and r_m the reaction rate of that reaction. In total, three reactions are included in the model. The first one is the endothermic methane steam reforming (MSR), in which methane reacts with steam to form hydrogen and carbon monoxide:

$$CH_4 + H_2O \rightleftharpoons 3H_2 + CO \tag{6}$$

Methane will be fully reformed at nominal stack operating temperatures, typically over 1100 K, thus it is assumed that all methane is fully reformed within the stack:

$$r_{\text{MSR}} = \dot{n}_{CH_4}^{\text{in}}. \tag{7}$$

However, it should be noted that this assumption is no longer realistic if the stack is to be operated at lower current densities and temperatures.

The second reaction considered is the water gas shift (WGS) reaction, in which carbon monoxide is converted to hydrogen:

$$CO + H_2O \rightleftharpoons H_2 + CO_2. \tag{8}$$

In contrast to the methane steam reforming reaction, the kinetics of the water gas shift reaction are often reported to be relatively fast. Therefore, its reaction quotient may be assumed equal to the equilibrium constant

$$Q_{\mathrm{WGS}} \equiv \frac{p_{H_2}\, p_{CO_2}}{p_{H_2O}\, p_{CO}} = K_{\mathrm{WGS}}. \tag{9}$$

The equilibrium constant K_{WGS} is a strong function of temperature and is calculated using the Gibbs free energy isotherm

$$K_{\mathrm{WGS}} = exp\left(-\frac{\Delta g_m^0}{\bar{R}T} \right). \tag{10}$$

Equations 9 and 10 are subsequently solved using a symbolic solver to calculate the partial pressures of hydrogen, carbon dioxide, carbon monoxide and steam. Since the total molar at the outlet is known, this can be used to calculate the WGS reaction rate

$$r_{\mathrm{WGS}} = \dot{n}_{CO}^{\mathrm{in}} - \frac{p_{CO}^{\mathrm{out}}}{p^{\mathrm{out}}} \dot{n}^{\mathrm{out}}. \tag{11}$$

The last reaction rate is the hydrogen oxidation reaction (HOR)

$$H_2 + \frac{1}{2} O_2 \Rightarrow H_2, \tag{12}$$

assuming only hydrogen is electrochemically oxidised. The hydrogen reaction rate is directly proportional to the stack current and the number of cells according to Faraday's law:

$$r_{\mathrm{HOR}} = \frac{I_{\mathrm{stack}} \cdot n_{\mathrm{cell}}}{2F}. \tag{13}$$

2.3 Electrochemistry

In the full model, the operating voltage of the SOFC is calculated by solving a spatially discretised current density distribution considering voltage differences resulting from activation, ohmic and concentration losses. As this implies solving a highly nonlinear system of equations, the electrochemistry is simplified in the reduced-order model.

The reversible or no loss voltage for a single cell is calculated from the Nernst equation

$$U_{\mathrm{Nernst}} = -\frac{\Delta \bar{g}^0}{2F} + \frac{\bar{R}T^{\mathrm{stack}}}{2F} ln\left(\frac{p_{H_2}\, \sqrt{p_{O_2}}}{p_{H_2O}} \right), \tag{14}$$

with $\Delta \bar{g}^0$ the Gibbs free energy of the HOR at reference conditions, F the Faraday constant and $\bar{R}$ the universal gas constant. The operating voltage of a single cell is then calculated by subtracting voltage losses. In the ROM, the various overpotential losses are simplified to a single, purely ohmic area specific resistance (R_{ASR}):

$$U_{\mathrm{cell}} = U_{\mathrm{Nernst}} - \frac{I_{\mathrm{stack}}}{A_{\mathrm{cell}}} R_{\mathrm{ASR}}. \tag{15}$$

The R_{ASR} may be assumed constant, calculated from a function or derived from experimental data. In this study, the ASR is fitted to operating maps generated with the high fidelity model.

The cells are electronically connected in series, such that the current is the same for all cells, the stack voltage follow from

$$U_{\mathrm{stack}} = n_{\mathrm{cell}} U_{\mathrm{cell}}, \tag{16}$$

and the stack power is subsequently calculated from:

$$P_{\mathrm{stack}} = U_{\mathrm{stack}} \cdot I_{\mathrm{stack}}. \tag{17}$$

3 Model verification

The implementation of the ROM is verified with the full high fidelity model to ensure that meaningful results are produced and it can thus be used for model-based control purposes. Therefore, characteristics of the SOFC stack calculated using the full model are presented in Section 3.1, and subsequently used to verify the ROM in Section 3.2. The ROM will be assessed in terms of numerical accuracy of the prediction of steady state output, stack outlet temperature $T_{\mathrm{stack}}^{\mathrm{out}}$ in particular, as well as the transient response to changes in model inputs.

Table 1: Inlet temperatures, stack current, fuel utilisation, air composition and fuel composition at nominal conditions.

Reference operating conditions	**Units**	**Value**
Fuel inlet temperature, T^{in}_{fuel}	[K]	1073.15
Air inlet temperature, T^{in}_{air}	[K]	923.15
Stack current, I_{stack}	[A]	27
Fuel utilisation, u_f	[-]	0.75

Air and fuel compositions (by volume)	
Air	O_2 (20%) N_2 (80%)
Fuel	H_2 (53%) H_2O (24%) CO (6%) CO_2 (9%) CH_4 (8%)

Table 2: Table comparing model outputs for reference operating points.

Parameter		Unit	High fidelity model	Reduced-order model	Error
$\dot{n}^{out}_{air}$	O_2	mol min^{-1}	1.097	1.097	0.00%
	N_2		5.074	5.075	0.02%
$\dot{n}^{out}_{fuel}$	CH_4	mol min^{-1}	0.00	0.00	0.00%
	CO_2		0.133	0.135	1.35%
	CO		0.036	0.035	3.96%
	H_2O		0.555	0.553	0.26%
	H_2		0.131	0.133	1.37%
T^{out}	air	K	1088.9	1088.6	0.03%
	fuel		1087.3		0.12%
U_{cell}		V	0.6538	0.6539	0.02%
P_{cell}		W	17.66	17.65	0.06%
Q_{loss}		W	4.11	4.106	0.1%

3.1 Full model characterisation

The full model is used to generate maps of relevant operating conditions for the stack. The results in Figure 2 show curves of constant air over stoichiometry (or oxygen utilisation), where the stack current increases from 10 A to 30 A. Figure 2a shows the stack power against the maximum temperature of the PEN structure calculated with the full model. Increasing the stack current or reducing the air stoichiometry results in a higher PEN temperature and, with exception of the highest temperatures, a higher stack power. However, it should be noted that the PEN temperature is restricted to about 1133 K in practice to avoid overheating. Therefore, the air flow needs to be adjusted accordingly to provide sufficient cooling.

The actual volumetric cathode air flow can be seen in Figure 2b, which increases with air stoichiometry and stack current. Figure 2b shows the resulting air outlet temperature as well, which is often used to control the stack temperature. While the temperature constrains can be managed by supplying excessive air flow, this is undesirable as it leads to a relatively high power consumption by the air compressor. In addition, lower stack temperatures lead to lower cell voltages, as shown in Figure 2c, and subsequently lower efficiencies.

3.2 Reduced-order model

The implementation of the ROM is verified in this section using the steady state operating points defined in the previous section. The outputs predicted with the ROM are compared to the full high fidelity model for the reference operating point defined in Table 1. The resulting outputs shown in Table 2 confirm that the outlet flows, temperatures, cell voltage, power and heat losses predicted with the ROM are resemble the full model results closely. A somewhat larger deviation, although still below 4%, can be seen with regard to the fuel composition at the outlet. This deviation seems to be a result of a slight change in the WGS equilibrium, which can be easily explained by the differences between the full and reduced-order model. While the full model is capable of predicting internal stack temperature that may locally exceed the outlet temperature, these are ignored due to the lumped parameter assumption in the ROM.

The ROM is based on the same physical principles as the full high fidelity model, but simplified. In order to reproduce the complicated electrochemistry implemented in the full model, values of the R_{ASR} in Equation (14)

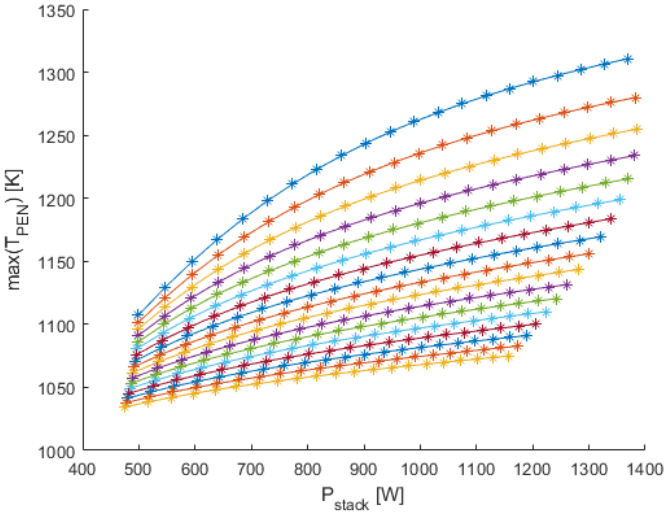

(a) Maximum PEN temperature and stack power.

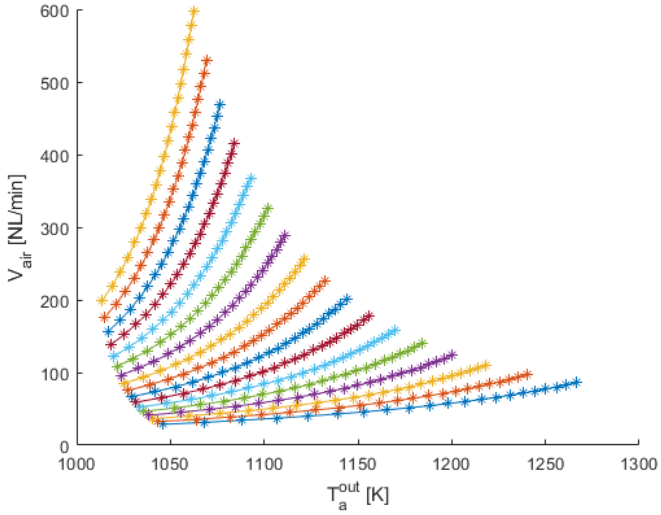

(b) Air outlet temperature and volumetric air flow.

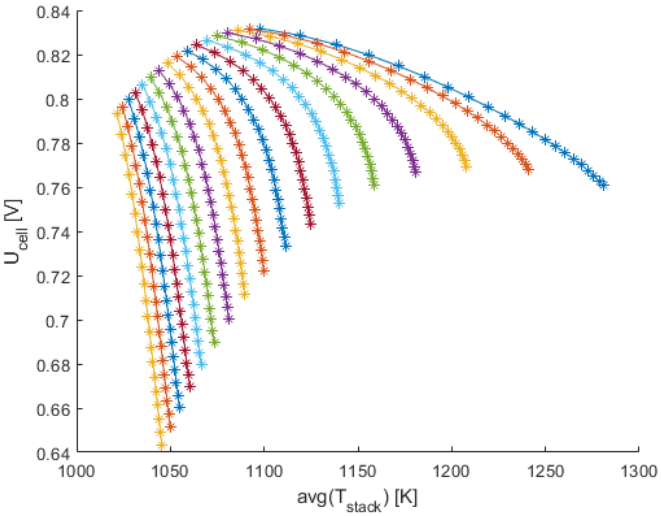

(c) Average stack temperature and cell voltage.

Figure 2: Operating maps of the SOFC stack generated with the full model. The different lines show steady-state operating points for different oxygen utilisations, varying from 5% to 50%. The stack current increases along the lines from 10 A to 30 A in steps of 1 A from top left to bottom right.

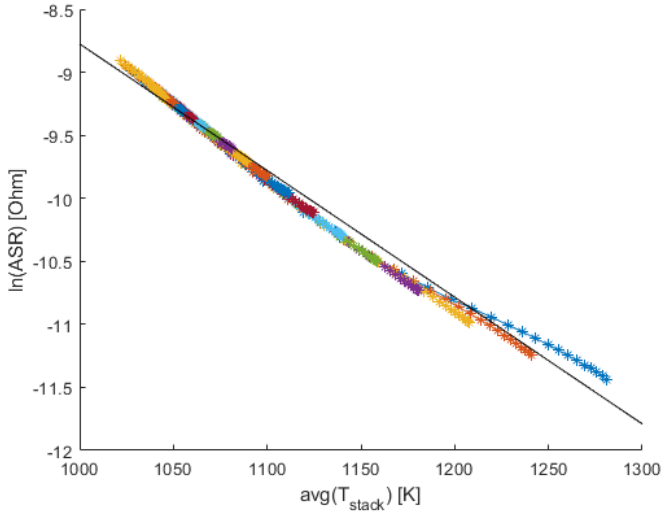

(a) Fitted ASR for the ROM.

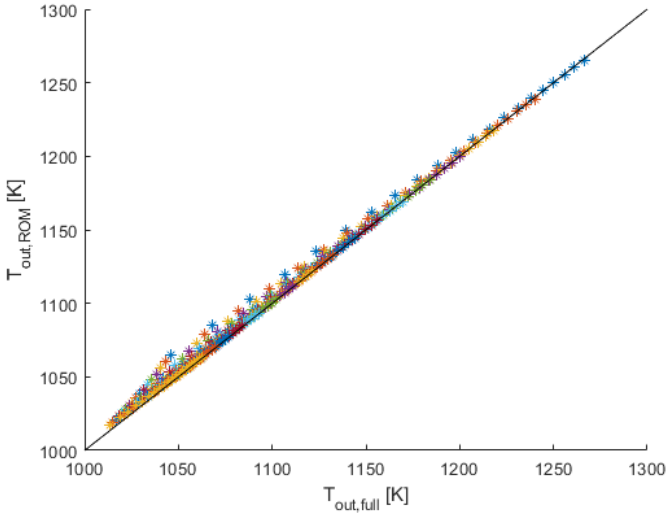

(b) Outlet temperatures for the full model vs ROM.

Figure 3: (a) ASR values fitted for the ROM for various average stack temperatures in the full model and (b) a comparison of outlet temperatures predicted with the full model and reduced-order model.

are fitted to the full model with the operating map provided in Section 3.1. Figure 3a plots the natural logarithm of the R_{ASR}, obtained by fitting the ROM to the simulated operating maps of the full model. The values are plotted against the average stack temperature calculated with the full model. The results confirm a more or less logarithmic dependency of R_{ASR} on the stack temperature, as is expected. A linear fit of the values reveals that such a dependency may be used as well if a small error is tolerable.

As the ROM is developed for thermal management purposes, its ability to predict the stack (outlet) temperature is most important. Figure 3b plots the air outlet temperature calculated with the full model against the lumped stack outlet temperature predicted by the ROM for the entire operating map. All points would coincide on the solid line for a perfect fit, which is the case for the majority of the points. However, deviations are observed especially at lower stack temperatures. This is most likely due to the assumption in the ROM that all methane is converted within the stack, which no longer holds at lower temperatures. However, this may be an acceptable error as it is not desirable to operate the stack at such low temperatures in practice.

4 Simulation experiments

The purpose of the ROM is the ability to predict the behaviour of an SOFC stack dynamically, and its thermal behaviour in particular. Therefore, three simulation experiments are defined in this section. These experiments involve ramping down and up three key model inputs, namely:

- Air inlet temperature (T_{air}^{in})
- Air inlet flow ($\dot{n}_{\text{air}}^{\text{in}}$)
- Stack current (I_{stack})

The results of the three test cases are shown in Figure 4, where the stack outlet temperature predicted by the ROM is compared to the air outlet temperature calculated with the high fidelity model.

Figure 4a shows the simulated response to ramping down the air inlet temperature from 1098.15 K to 298.15 K over a period of 1000 seconds and holding it for 5000 seconds before ramping it back up. The average stack temperature calculated with the full model is shown as well. While the response of the outlet temperature is similar for the two models, the ROM reaches a lower temperature and responds faster than the full model.

The lower steady state temperature predicted by the ROM can be explained by the fact that all methane is assumed to be reformed, even for temperatures as low as 298.15 K, while in reality hardly any methane is expected to be reformed at these temperatures. The delayed response of the air outlet temperature in the full high fidelity model is likely a result of the spatial discretisation of that model and emphasizes the need for such high fidelity models for accurate simulation of thermal behaviour, as these dynamics are difficult to predict with the common lumped modelling approaches. However, such models are still capable of predicting the average stack behaviour, which is apparent when comparing the outlet temperature predicted by the ROM to the average stack temperature calculated with the full model.

Figure 4b and Figure 4c show a similar comparison for doubling the air flow rate and the decreasing the stack current from 27 A to 0 A in the same time frame. Similar to the first case, the ROM under predicts the outlet temperature as the stack temperature decreases, probably because complete internal methane reforming is still assumed. Interestingly, the response of the ROM to changes in these parameters seems to be more accurate than the change in air temperature. All in all, the behaviour of the ROM is judged sufficient for thermal management purposes.

The results are ideally compared to experimental data as well. However, such data is scarce in literature and was not available for the system simulated in this study. Obtaining experimental data for dynamic ISM operation is thus a key objective of future studies and a necessity prior to implementation in the system of interest. Nonetheless, the time scales encountered in [13] were found to match those reported by the manufacturer. Therefore, both the high fidelity model and ROM should be sufficient to develop and evaluate different control strategies. These may eventually be taylored to specific designs and validated with hardware-in-the-loop experiments.

5 Preliminaries on model predictive SOFC control using the reduced-order model

Section 2 presented the derivation of a reduced-order model from a high fidelity model, which was subsequently verified and validated in Sections 3 and 4, respectively. Such model encompasses differential and algebraic equations of different nature, for which a summary is provided below:

- Energy balance: equations (3) and (4)
- Mass balance: equations (5), (7), (9), (10), (11) and (13)
- Electrochemistry: equations (14), (15), (16) and (17)

Contrary to the original high fidelity model, the reduced-order model is amenable to real-time implementations. Therefore, it can be used as prediction model to compute a control law that ensures satisfactory system operation. As a first step, manipulated and controlled variables are identified below:

- Manipulated variables (inputs): air and fuel inlet flows and temperatures, and stack current.
- Controlled variables (states): air and fuel outlet flows, outlet (stack) temperature, heat loss, stack voltage and power.

The input and state vectors, denoted in standard control notation with $\mathbf{u}$ and $\mathbf{x}$, respectively, are given by

$$\mathbf{u} = \left[\dot{n}_{O_2}^{\text{in}}\ \dot{n}_{N_2}^{\text{in}}\ \dot{n}_{CH_4}^{\text{in}}\ \dot{n}_{CO_2}^{\text{in}}\ \dot{n}_{CO}^{\text{in}}\ \dot{n}_{H_2O}^{\text{in}}\ \dot{n}_{H_2}^{\text{in}}\ T_{\text{air}}^{\text{in}}\ T_{\text{fuel}}^{\text{in}}\ I_{\text{stack}}\right]^{\intercal}, \tag{18a}$$

$$\mathbf{x} = \left[\dot{n}_{O_2}^{\text{out}}\ \dot{n}_{N_2}^{\text{out}}\ \dot{n}_{CH_4}^{\text{out}}\ \dot{n}_{CO_2}^{\text{out}}\ \dot{n}_{CO}^{\text{out}}\ \dot{n}_{H_2O}^{\text{out}}\ \dot{n}_{H_2}^{\text{out}}\ T_{\text{stack}}\ \dot{Q}_{\text{loss}}\ U_{\text{stack}}\ P_{\text{stack}}\right]^{\intercal}, \tag{18b}$$

where $^{\intercal}$ denotes vector transposition.

SOFC operation for the targeted application aims to fulfil a set of performance objectives:

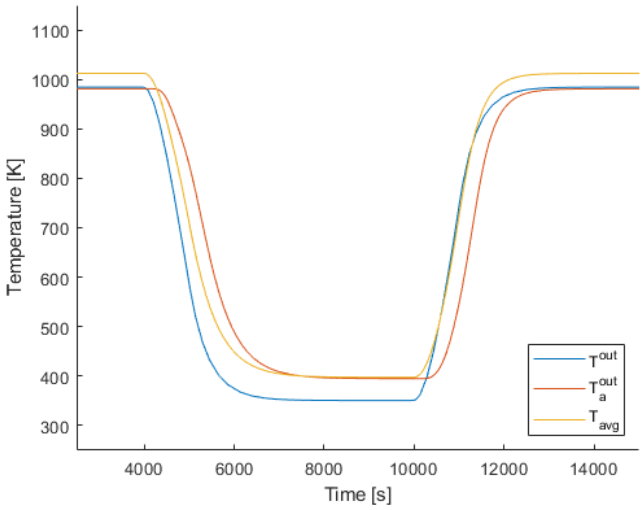

(a) Response to air temperature ramp.

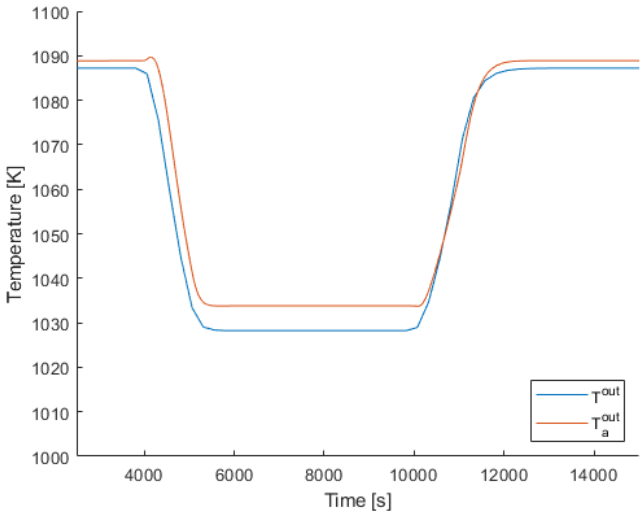

(b) Response to air flow ramp.

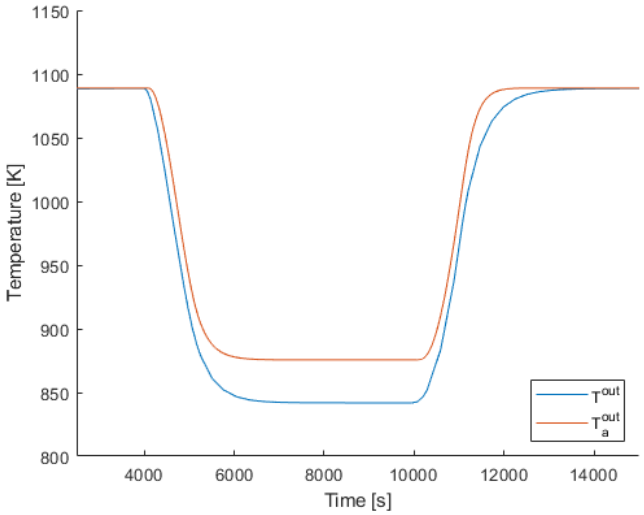

(c) Response to current ramp.

Figure 4: Dynamic simulation results. Responses to a change (ramp in (a) air overstoichiometry, (b) stack current and (c) air inlet temperature, showing the air outlet temperature of the full model (T_a^{out}), the (lumped) outlet temperature of the ROM (T^{out}) and the average stack temperature in the full model (T_{avg}).

- Supply the required power as fast as possible with minimal error and no overheating.
- Maximize efficiency by ensuring that the SOFC operates within a certain region.
- Achieve the previous objectives with minimal control effort, i.e., minimal current, air and fuel flows.
- Minimize rate of change of control signals, which has a direct effect on reducing equipment deterioration.

At the same time, certain physical and operational constraints must be observed during system operation:

- Ensure that the stack temperature remains within safety bounds to prevent, e.g., sintering, melting and thermal stress. This is a *hard* constraint, and cannot be violated.
- Ensure that the stack temperature remains within efficiency bounds (smaller temperature interval within safety bounds) as much as possible. This is a *soft* constraint, which means that temperatures are allowed to be outside of this interval (although its occurrence should be penalized).

With all this in mind, a suitable control strategy must be selected. Three main features are sought: (i) the possibility to use the reduced-order model as prediction model, (ii) the simultaneous consideration of multiple (and possibly conflicting) performance objectives, and (iii) the capability to deal with input and state constraints. One of the most popular model-based control approaches is model predictive control (MPC), which employs a dynamic model of the process to predict the future effect of inputs on the system within the prediction horizon, and select the values that yield the optimal performance [1]. Moreover, the receding horizon strategy, whereby only the first value of the sequence of optimal inputs is applied, transforms the original open-loop control problem into a closed-loop one. In this way, the most recent information can be exploited at each sampling instant, and mismatches can be corrected for [9].

6 Conclusions

In this paper, a ROM of an SOFC stack is developed for model-based control purposes. The ROM reduces the number of dynamic states from 968 in a high fidelity model to only the lumped stack temperature. In addition, the electrochemical model is simplified to omit solving a highly non-linear and coupled system of equations. For this purpose, the ASR is fitted to the high fidelity model. These simplifications enable faster than real-time evaluation of the SOFC behaviour, suitable for model-based control. The ROM is verified with the full model, and the response to transients in the inlet air temperature, air flow and stack current compared. The results confirm that the ROM is able to predict the SOFC stack temperatures with sufficient accuracy for model-based control purposes, for which a framework is presented. Model validation with experimental data and its application in an MPC strategy is ongoing and results will be published in future work.

Acknowledgements

This research is supported by the project *"GasDrive: Minimizing emissions and energy losses at sea with LNG combined prime movers, underwater exhausts and nano hull materials"* (project 14504) of the Netherlands Organisation for Scientific Research (NWO), domain Applied and Engineering Sciences (TTW), the project *"NoMES: Novel and Minimized Emissions Shipping "* of the Nederland Maritiem Land (NML) and the Researchlab Autonomous Shipping (RAS) of Delft University of Technology.

References

[1] E. F. Camacho and C. Bordons. *Model Predictive Control*. Springer, London, 1998.

[2] G. D'Andrea, M. Gandiglio, A. Lanzini, and M. Santarelli. Dynamic model with experimental validation of a biogas-fed SOFC plant. *Energy Conversion and Management*, 135:21–34, 2017.

[3] M. Fardadi, D. F. McLarty, and F. Jabbari. Investigation of thermal control for different sofc flow geometries. *Applied Energy*, 178:43–55, 2016.

[4] M. Gandiglio, A. Lanzini, and M. Santarelli. Large stationary solid oxide fuel cell (SOFC) power plants. In *Modeling, Design, Construction, and Operation of Power Generators with Solid Oxide Fuel Cells*, pages 233–261. Springer, 2018.

[5] S. Hosseini, V. A. Danilov, P. Vijay, and M. O. Tadé. Improved tank in series model for the planar solid oxide fuel cell. *Industrial & Engineering Chemistry Research*, 50(2):1056–1069, 2010.

[6] S. Kluge, O. Posdziech, B. E. Mai, and J. Lawrence. Performance Map of the Staxera Integrated Stack Module with Partly Internal Reforming. *ECS Transactions*, 25(2):247–256, 2009.

[7] W. G. Mallard. National Institute of Standards and Technology Chemistry Web Book, 2003.

[8] R. Payne, J. Love, and M. Kah. Generating electricity at 60% electrical efficiency from 1-2 kWe SOFC products. *ECS Transactions*, 25(2):231–239, 2009.

[9] J. B. Rawlings and D. Q. Mayne. *Model Predictive Control: Theory and Design*. Nob Hill Pub. Madison, Wisconsin, 2009.

[10] C. H. Shomate. A method for evaluating and correlating thermodynamic data. *The Journal of Physical Chemistry*, 58(4):368–372, 1954.

[11] L. van Biert. *Solid Oxide Fuel Cells for Ships: System integration concepts with reforming and thermal cycles*. PhD thesis, Delft University of Technology, 2020.

[12] L. van Biert, M. Godjevac, K. Visser, and P. V. Aravind. A review of fuel cell systems for maritime applications. *Journal of Power Sources*, 327:345–364, 2016.

[13] L. van Biert, M. Godjevac, K. Visser, and P. V. Aravind. Dynamic modelling of a direct internal reforming solid oxide fuel cell stack based on single cell experiments. *Applied Energy*, 250:976–990, 2019.

[14] L. van Biert, K. Visser, and P. Aravind. A comparison of steam reforming concepts in solid oxide fuel cell systems. *Applied Energy*, 264:114748, 2020.

[15] Z. Zeng, Y. Qian, Y. Zhang, C. Hao, D. Dan, and W. Zhuge. A review of heat transfer and thermal management methods for temperature gradient reduction in solid oxide fuel cell (sofc) stacks. *Applied Energy*, 280:115899, 2020.